The EMBO Journal (2006) 25, 24–33 | © 2006 European Molecular Biology Organization | All Rights Reserved 0261-4189/06
www.embojournal.org

THE
EMBO
JOURNAL

Ion-binding properties of the ClC chloride selectivity filter

Séverine Lobet and Raimund Dutzler*

Department of Biochemistry, University of Zürich, Zürich, Switzerland

The ClC channels are members of a large protein family of chloride (Cl^-) channels and secondary active Cl^- transporters. Despite their diverse functions, the transmembrane architecture within the family is conserved. Here we present a crystallographic study on the ion-binding properties of the ClC selectivity filter in the close homolog from *Escherichia coli* (EcClC). The ClC selectivity filter contains three ion-binding sites that bridge the extra- and intracellular solutions. The sites bind Cl^- ions with mM affinity. Despite their close proximity within the filter, the three sites can be occupied simultaneously. The ion-binding properties are found conserved from the bacterial transporter EcClC to the human Cl^- channel ClC-1, suggesting a close functional link between ion permeation in the channels and active transport in the transporters. In resemblance to K^+ channels, ions permeate the ClC channel in a single file, with mutual repulsion between the ions fostering rapid conduction.

The EMBO Journal (2006) **25,** 24–33. doi:10.1038/sj.emboj.7600909; Published online 8 December 2005
Subject Categories: membranes & transport; structural biology
Keywords: ClC chloride channels and transporters; ion selectivity; ion transport; selectivity filter; X-ray crystallography

Introduction

The flux of ions across cellular membranes is the basis for important physiological processes as electrical signaling, control of the cell volume and ion homeostasis. Transmembrane ion transport presents an energetic challenge, since it requires the balance of large and long-range electrostatic interactions (Parsegian, 1969). The maintenance of the energetic balance is particularly important for ion channels, which specifically allow the permeation of ions at very high rates. The structures of ion channel proteins reveal the mechanisms employed to keep the strict energetic balance (Doyle *et al*, 1998; Zhou and MacKinnon, 2004). The mechanisms include ion–protein interactions in extended low-affinity ion-binding sites and the binding of multiple ions, which, due to their mutual electrostatic repulsion, lower the barrier for dissociation from the binding sites (Hille and Schwarz, 1978; Morais-Cabral *et al*, 2001; Zhou and MacKinnon, 2003). The principles of ion conduction are now well established for the large family of K^+ channels; they remain less clear, however, for other ion channel proteins.

Next to K^+ channels, the ClC Cl^- channels are the second class of selective ion channel proteins, with a known structural scaffold (Dutzler *et al*, 2002, 2003). ClC channels constitute a large protein family, which is found from bacteria to mammals. Their physiological importance is evident from a broad range of tasks and from their link to various diseases (Jentsch *et al*, 2002). In sequence and structure the ClC channels are not related to K^+ channels or any other class of ion channel proteins, and in their function they exhibit a unique feature: while several characterized eukaryotic family members residing in the plasma membrane work as Cl^- selective ion channels with a complex gating behavior, a close prokaryotic homolog from *Escherichia coli* (EcClC) and several eukaryotic family members localized in intracellular organelles function as an H^+/Cl^- exchanger, where the flux of Cl^- is coupled to the flux of protons in the opposite direction (White and Miller, 1979; Accardi and Miller, 2004; Picollo and Pusch, 2005; Scheel *et al*, 2005).

The crystal structure of EcClC was determined by X-ray crystallography (Dutzler *et al*, 2002, 2003). It provides insight into the structural organization of the ClC family and reveals the chemical basis for anion selectivity. EcClC is a homodimer of structurally identical subunits, with each subunit containing an ion translocation pore (Figure 1A). The topology of the subunit is complex; it consists of two roughly repeated halves, which span the membrane with opposite orientation. This antiparallel architecture defines a selectivity filter in the center of the membrane within the 15 Å neck of an hourglass-like-shaped pore. Cl^- ions bind to three distinct sites in the selectivity filter and interact with partial charges from hydroxyl groups of amino-acid side chains and with backbone amide NH groups, most of which are located at the N-terminus of α-helices (Figure 1B).

The ion-binding sites were identified by X-ray crystallography, making use of the property of ClC channels to bind and conduct Br^- nearly, as well as Cl^- (Rychkov *et al*, 1998; Dutzler *et al*, 2002, 2003; Accardi *et al*, 2004). The data reveal where the ions are binding; they do not, however, allow to distinguish whether all the three binding sites can be occupied at the same time or whether the structure represents an ensemble of structures with one or two ions bound.

To date, the detailed mechanisms for ion conduction in ClC channels and for transport in EcClC and other H^+/Cl^- transporters are still unclear. There is, however, good evidence that both functional branches channels and transporters are similar in structure and have conserved modes of ion binding (Chen and Chen, 2003; Estevez *et al*, 2003; Engh and Maduke, 2005). To get insight into both mechanisms, permeation and transport, it is important to understand the ion-binding properties of the selectivity filter. Here we use a crystallographic approach to address the following questions: how many ions bind to the selectivity filter at the same time;

*Corresponding author. Department of Biochemistry, University of Zürich, Winterthurer Strasse 190, 8057 Zürich, Switzerland.
Tel.: +41 44 635 6550; Fax: +41 44 635 6834;
E-mail: dutzler@bioc.unizh.ch

Received: 6 September 2005; accepted: 17 November 2005; published online: 8 December 2005

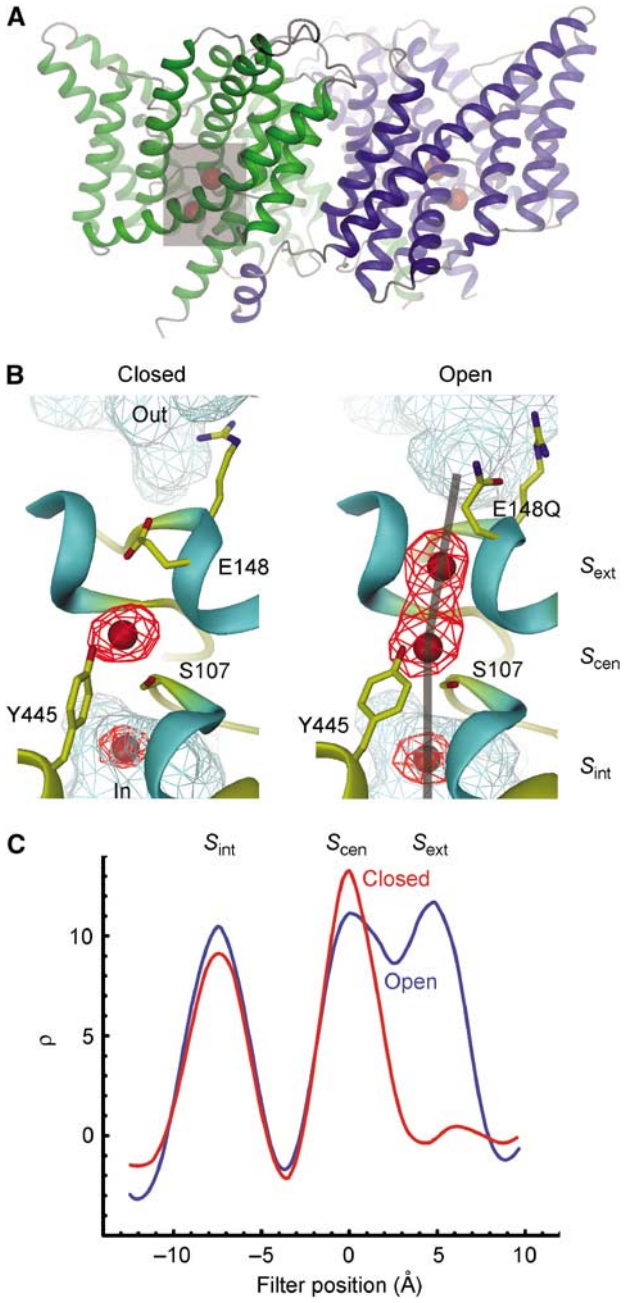

Figure 1 Structure and ion-binding properties of the EcClC selectivity filter. (**A**) View of a ribbon representation of the EcClC dimer from within the membrane. The subunits are colored in green and blue. The ions are represented as red spheres. The region of the selectivity filter in one subunit is indicated by a transparent gray box. (**B**) Selectivity filter of wtEcClC (closed) and the EcClC mutant E148Q (open) viewed from the dimer interface. The protein backbone is shown as a ribbon, with selected residues as sticks. The N-terminal ends of α-helices are colored in cyan. The ions are represented as red spheres. The Br^- anomalous difference density (contoured at 6σ) is shown superimposed (red). The path for sampling the anomalous difference density is shown as gray lines (open). Aqueous cavities from the extracellular solution (out) and intracellular solution (in) are shown as cyan mesh. The ion-binding sites are labeled. (A) and (B) were prepared with DINO (www.dino3d.org). (**C**) One-dimensional anomalous difference electron density in the selectivity filter at high Br^- concentration. The density (ρ) is plotted in units of its standard deviation. The filter position is shown relative to S_{cen}. The curve for the 'open conformation' is colored in blue, the curve for the 'closed conformation' in red.

how selective are the ion-binding sites for the related anions Cl^- and Br^-; what are their affinities for the two ions and does the protein change its conformation in the absence of bound ions.

Results

Two conformations of the ClC selectivity filter

Presently, we know the structure of the EcClC selectivity filter in two conformations. Figure 1B shows a blowup of the two conformations in wt EcClC and in the mutant E148Q. The filter contains three ion-binding sites, which were previously named S_{int}, S_{cen} and S_{ext} (Dutzler *et al*, 2003). The ion-binding sites bridge the two aqueous vestibules approaching the narrow selectivity filter from both sides of the membrane. Only S_{int} and S_{cen} are occupied by ions in the wt structure, where the negatively charged side chain of the conserved Glu 148 residue binds to S_{ext}, akin to a tethered anion. A mutation of this glutamate residue to glutamine prevents binding of the side chain to S_{ext} and allows for binding of an ion instead (Dutzler *et al*, 2003). As shown by electrophysiology, the mutation of the respective Glu residue in the Cl^- channel ClC-0 prevents closing of the pore (Dutzler *et al*, 2003; Traverso *et al*, 2003). In EcClC the same mutation abolishes H^+ transport, while still allowing the permeation of Cl^- (Accardi and Miller, 2004). The ion binding to S_{ext} in the E148Q mutant and the effects on gating and on transport are indicative for a functional relationship between the two mechanisms and let us propose that the two structures resemble the open and closed states of the selectivity filter of a ClC channel with respect to ion binding. Therefore, in our study, the structure of wt EcClC serves as a model of the ClC selectivity filter in a nonconductive state ('closed conformation') and the mutant E148Q as a model for a conductive state ('open conformation') (Dutzler *et al*, 2003). Both conformations also represent likely intermediates along the transport cycle of the H^+/Cl^- transporters. It has to be pointed out that to date the 'open conformation' has only been observed in mutants of the E148 residue and was never seen in the wt protein irrespectively of the pH or the ion concentration during crystallization. It might well be that this conformation is energetically not favorable in wt EcClC and consequently not populated. The model of the 'open conformation' is for that reason approximative.

Measuring ion binding by crystallography

To gain insight into the ion-binding properties of the ClC selectivity filter, we make use of a crystal form of EcClC in complex with Fab fragments from a monoclonal antibody raised against the protein (Dutzler *et al*, 2003). The Fab fragments bind remotely from the selectivity filter and do not interfere with ion binding. We quantify ion binding by growing our crystals in solutions containing Br^- ions and by collecting our data sets at a wavelength corresponding to the anomalous absorption edge of Br^-. We use Br^-, since the anomalous absorption edge of Cl^- is not in the accessible wavelength range of synchrotron sources. In functional experiments, Br^- has been shown to be a good analog for Cl^- (Accardi *et al*, 2004).

Figure 1C shows the one-dimensional electron density distribution in the ClC selectivity filter measured from a normalized $F^+_{Br}-F^-_{Br}$ anomalous difference map. The

normalization allows us to compare data sets collected from crystals grown at different Br^- concentrations. The histogram of the electron density follows a Gaussian distribution. During normalization, the average of this distribution is subtracted and the corrected density is subsequently scaled by the reciprocal value of the standard deviation (Supplementary Figure 1). The electron density of the 'open conformation' has three peaks, each peak corresponding to a Br^- ion in its respective ion-binding site. The adjacent peaks in S_{int}, S_{cen} and S_{ext} are separated by 7 and 5 Å, respectively. The larger separation between S_{int} and S_{cen} is partially due to the side chain of Ser107, which coordinates the ion in S_{cen} and is located between the two ion-binding sites, while the ions in binding sites S_{cen} and S_{ext} are nearly in 'van der Waals' distance and would come very close if the sites are occupied at the same time (Figure 1B and C). In the 'closed conformation', the distance between ions bound to S_{int} and S_{cen} is the same, while the peak in S_{ext} is absent (Figure 1C).

Both peak height and area in the one-dimensional anomalous difference density depend on the fraction of the binding sites occupied by a Br^- ion, on the mobility of the ion (as measured by the atomic *b*-factor) and on the wavelength of the X-ray beam (Supplementary Figure 2). The signal is robust; it was found to be relatively insensitive to the resolution of the data sets and varies little with the stage of refinement (Supplementary Figure 1B and C). The largest error is introduced by comparing electron densities collected from different crystals, and is due to differences in data quality and characteristics of the X-ray beam. To minimize this error, all data sets used in this study were collected at the same synchrotron beamline. Each data set allows for two independent measurements from the two subunits in the asymmetric unit, and for most concentrations data sets from two crystals were collected. The errors listed in Table II and Supplementary Table II are the standard deviations of the mean value in cases where the average was taken between the four sites present in two data sets or describe the range of values in the two subunits for concentrations where data were only collected from one crystal. In our study we use both, the measured peak height (Table I) and the fitted peak area (Supplementary Table I), as a measure of ion occupancy in the binding site, assuming that the mobility of bound ions remains the same at all ion concentrations. The fit of a sum of Gaussians to the one-dimensional electron density distribution shows that the peak heights in the electron density are not significantly influenced by the density of the adjacent ion (Supplementary Figure 2D). Both values, measured peak height and fitted peak area, show a linear correlation at different ion concentrations and are therefore both valid approximations of the three-dimensional electron density (Supplementary Figures 2C, E and 3, Supplementary Table II). The peak heights are used as a measure of the electron density and of the fits in the main text because they allow for a better approximation of ion occupancy at low Br^- concentration, where the sites are only partially occupied. The 31 data sets used in this study were collected from crystals grown in a pH range between 6.5 and 9.5. The pH did not have any observable effect on the structure or the ion-binding properties of the protein. All crystals were diffracting to a resolution between 3.1 and 4.0 Å, with most of the data sets being at a resolution of 3.6 Å or higher (Table I). A resolution cutoff of $I/\sigma I > 5$ was applied for calculating the Br^- anomalous difference maps. The upper resolution of the various difference maps ranges between 3.2 and 4.2 Å, features like the peak height and the spacing between the peaks are found preserved (Supplementary Figure 1 B and C).

Ion occupancy in the selectivity filter

The peaks in the anomalous difference density saturate at high Br^- concentration. Due to the limited resolution, however, we cannot make a measure of the absolute occupancy. It is possible that the close proximity of the ion-binding sites and the resulting strong electrostatic repulsion between the ions prevent the three binding sites in the filter to be occupied at the same time. In this case, the peaks in the anomalous difference density correspond to an ensemble of molecules with partially occupied sites.

To address the question of ion occupancy in the selectivity filter, we constructed a mutant where two of the three ion-binding sites are abolished. In case that in the 'open conformation' a site is, due to the electrostatic repulsion between adjacent ions, only partially occupied, we would expect it to get fully occupied, if the neighboring ion binding sites are empty, and we therefore expect the peak in the anomalous density to increase.

In the triple mutant Y445A/S107A/E148Q (which for simplicity is called TRPL), two side chains, which interact with the bound ion in S_{cen}, are truncated to alanine. The mutant is otherwise very similar to the 'open conformation' (Figure 2A). Surprisingly, next to the peak in S_{cen} also the peak in S_{int} is absent (Table I, Figure 2A and C). Despite the three mutations, TRPL facilitates selective chloride uptake into vesicles (Figure 2B). The electron density ($2F_o-F_c$) of the mutant at 3.5 Å resolution shows S_{ext} unperturbed, with no noticeable changes in the overall structure (Figure 2A). As we will show later, for crystals grown at high ion concentration, the Br^- ion concentration in the crystallization solution (250 mM) is 50 times excess of the K_D for Br^- binding to S_{ext} in the 'open conformation'. Strong peaks of bound ions are also seen in a crystal grown in 100 mM Br^- (Figure 2A). It can therefore safely be assumed that the single binding site in TRPL is fully occupied. Measurements from two crystals at high Br^- concentration independently show an electron density distribution, which is very similar to that of S_{ext} in the 'open conformation' (Figure 2C, Tables I and II, Supplementary Tables I and II). Since the anomalous difference density for S_{ext} in TRPL is not increased, we conclude that all the three ion-binding sites are fully occupied in the 'open conformation'.

Br^- affinity of the ion-binding sites

To estimate the affinity of the individual ion-binding sites, we crystallized the protein at various Br^- concentrations, ranging from high Br^- concentrations to conditions which completely lack halide ions. For low halide ion concentrations, we had to identify a novel crystal form that grows in the absence of ions that bind to the EcClC selectivity filter (see Materials and methods). Figure 3A shows the anomalous Br^- difference density in the 'open conformation' at Br^- concentrations ranging from 250 to 1 mM. The concentration refers in all cases to the ion concentration in the crystallization solution after equilibration. A decrease in the peak size reflects the depletion of the binding site of ions. This depletion occurs for the three binding sites at different ion

Table I Summary of data collection and refinement statistics

[Br^-] (mM)	pH	Resolution[a]	Mos.[b]	R_{sym}[c] (%)	R/R_{free}[d]	ρA[e] ($S_i/S_c/S_e$)	ρB[e] ($S_i/S_c/S_e$)
'Open conformation' affinity							
0	9.5	3.4	0.9	12.1	29.8 (32.5)	2.5/1.9/2.3	2.5/2.7/1.9
0[f]	8.5	3.1	1.2	8.3	33.4 (35.2)	1.3/2.5/2.3	1.3/2.0/1.4
1	6.5	3.9 (4.2)	1.1	13.1	33.2 (34.6)	0.4/0.6/0.2	1.6/1.0/0.6
1	9.5	3.9 (4.1)	0.5	11.1	33.2 (33.4)	1.2/1.2/3.2	0.2/1.2/2.4
5	9.5	3.8 (4.2)	0.8	12.5	33.7 (35.1)	4.1/3.0/3.1	1.1/4.7/4.5
5	8.5	3.3 (3.7)	1.3	8.3	32.8 (35.1)	4.2/4.4/5.4	3.7/2.4/6.8
10	9.5	3.4 (3.7)	0.8	10.4	29.6 (31.5)	3.5/5.8/9.7	3.7/3.6/9.3
10	9.5	3.5 (3.8)	1.0	9.7	30.9 (31.9)	4.7/3.7/8.1	4.8/5.1/11.3
25	9.5	3.8 (4.1)	0.5	12.0	35.6 (35.2)	3.8/8.8/9.7	3.3/7.0/10.3
25	7.5	3.1 (3.2)	0.7	7.6	31.7 (33.2)	9.7/14.1/17.0	7.7/12.5/17.0
75	7.5	3.7 (4.1)	0.9	9.4	34.9 (34.8)	7.2/11.2/14.0	8.2/13.3/14.6
250	9.5	3.9 (4.2)	1.9	10.0	38.1 (39.9)	10.5/11.1/11.7	9.9/8.4/9.3
250	7.5	3.3 (3.4)	0.9	8.1	34.7 (37.6)	11.2/16.8/16.4	8.7/7.7/10.2
'Closed conformation' affinity							
0	9.5	3.5 (3.9)	1.2	11.1	32.4 (33.7)	1.2/0.9/–	−0.5/1.0/–
1[f]	9.5	3.2 (3.7)	1.1	10.2	26.3 (31.4)	0.9/0.8/–	2.0/1.2/–
5	6.5	3.3 (3.6)	0.6	8.0	29.3 (31.1)	3.1/5.9/–	3.8/7.1/–
5	9.5	3.2 (3.5)	0.4	8.2	30.1 (31.7)	2.9/5.7/–	1.7/5.0/–
25	6.5	3.5 (3.8)	0.6	10.3	29.4 (30.9)	5.4/11.1/–	4.8/11.1/–
400	9.5	3.6 (3.8)	0.9	10.6	36.6 (37.7)	9.1/13.3/–	8.2/9.5/–
TRPL							
250	9.5	3.8 (4.2)	0.5	10.2	35.2 (38.3)	–/–/11.5	–/–/10.5
250	6.5	3.8 (4.2)	1.1	9.1	36.1 (37.9)	–/–/11.2	–/–/7.5
100[f]	9.5	3.5 (3.9)	0.8	8.6	25.8 (29.5)	–/–/8.0	–/–/6.4
$Br^-/Br^- + Cl^-$ (%)	pH	Resolution[a]	mos.	R_{sym} (%)	R/R_{free}[b]	ρ A[c] $S_i/S_c/S_e$	ρ B[c] $S_i/S_c/S_e$
'Open conformation' selectivity							
75	8.5	3.5 (3.8)	1.1	7.4	34.5 (37.7)	9.2/2.7/7.9	9.0/3.3/11.0
75	7.5	3.6 (4.0)	0.9	10.6	34.3 (36.5)	8.1/6.4/8.8	4.3/3.8/4.6
50	8.5	3.1 (3.4)	1.3	9.3	31.3 (34.9)	5.8/1.7/2.9	8.0/4.0/4.6
50	8.5	3.6 (4.0)	1.0	11.8	32.7 (35.9)	6.5/0.1/3.7	5.9/2.0/4.8
25	8.5	3.7 (4.1)	1.9	11.4	37.6 (38.3)	2.5/1.9/3.0	2.5/0.5/1.4
25	7.5	3.2 (3.5)	0.8	10.1	34.4 (36.9)	3.3/2.2/3.6	3.7/0.9/3.0
'Closed conformation' selectivity							
75	8.5	3.6 (3.8)	0.9	9.0	31.2 (33.8)	10/6.2/–	9.9/7.3/–
50	7.5	4.0 (4.2)	1.29	9.9	37.3 (38.9)	5.4/3.5/–	5.4/3.4/–
25	7.5	3.7 (4.1)	0.69	10.2	35.7 (35.9)	2.4/2.7/–	3.9/1.5/–

[a]Data were included to an overall $I/\sigma I$ of 2.0. Structures were refined using the entire resolution range. Data in parenthesis show the resolution at a cutoff of $I/\sigma I$ of 5. Anomalous difference densities were calculated to this resolution. Most data sets are >95% complete, the lowest completeness in any data set is 89%.
[b]Mosaicity.
[c]$R_{sym} = \sum|I_i - \langle I_i \rangle| / \sum|I_i|$, where I_i is the scaled intensity of the ith measurement and $\langle I_i \rangle$ is the mean intensity for that reflection.
[d]R/R_{free}: $R = \sum||F_o| - |F_c|| / \sum|F_o|$, where F_o and F_c are the observed and calculated structure factor amplitudes, respectively. R_{free} values are listed in parenthesis. R_{free} was calculated from 5% of the reflections, which were not included in refinement. The same set of reflections was previously used for the refinement of the structures 1OTS and 1OTU, which served as starting models for refinement, and for each data set in this study.
[e]ρA, ρB: Peak heights in the normalized anomalous difference density in subunits A and B. The peaks are listed for S_{int}, S_{cen} and S_{ext}. The values were used for the averages listed in Table II.
[f]Structures and structure factors have been deposited with the Protein Data Bank under the accession codes 2EXW (wtEcClC 1 mM Br^-), 2EXY (EcClC E148Q 0 mM Br^-) and 2EZ0 (EcClC S107A/E148Q/Y445A 100 mM Br^-).

concentrations: While the anomalous difference density in S_{int} already vanishes below 25 mM Br^-, the density in S_{cen} approaches its half-maximum value between 25 and 10 mM Br^-. The electron density in S_{ext} remains strong at low ion concentration, still being close to its maximum at 10 mM Br^-. The anomalous difference electron density of the 'closed conformation' shows similar features (Figure 3B). The density in S_{int} reaches its half-maximum value at 25 mM Br^-, while the peak in S_{cen} is still above half of its size at 5 mM Br^-. In both conformations the curves do not show density at 1 mM Br^-, indicating that no ions are bound to the selectivity filter.

The binding affinities can be estimated from the anomalous density at various ion concentrations (Table I). The respective peak heights were averaged between the two subunits in the asymmetric unit and in many cases also between data sets measured from different crystals. The Br^- affinity was determined by a fit of the average densities to the following equation (Figure 3C and D):

$$\rho = (\rho_{max} - \rho_{min})/(K_D/[Br^-] + 1) + \rho_{min} \quad (1)$$

All three binding sites bind Br^- ions with mM affinity (Figure 3C and D, Table II). In the 'open conformation' S_{ext} has the highest affinity with a K_D of 6 mM. The K_D values of

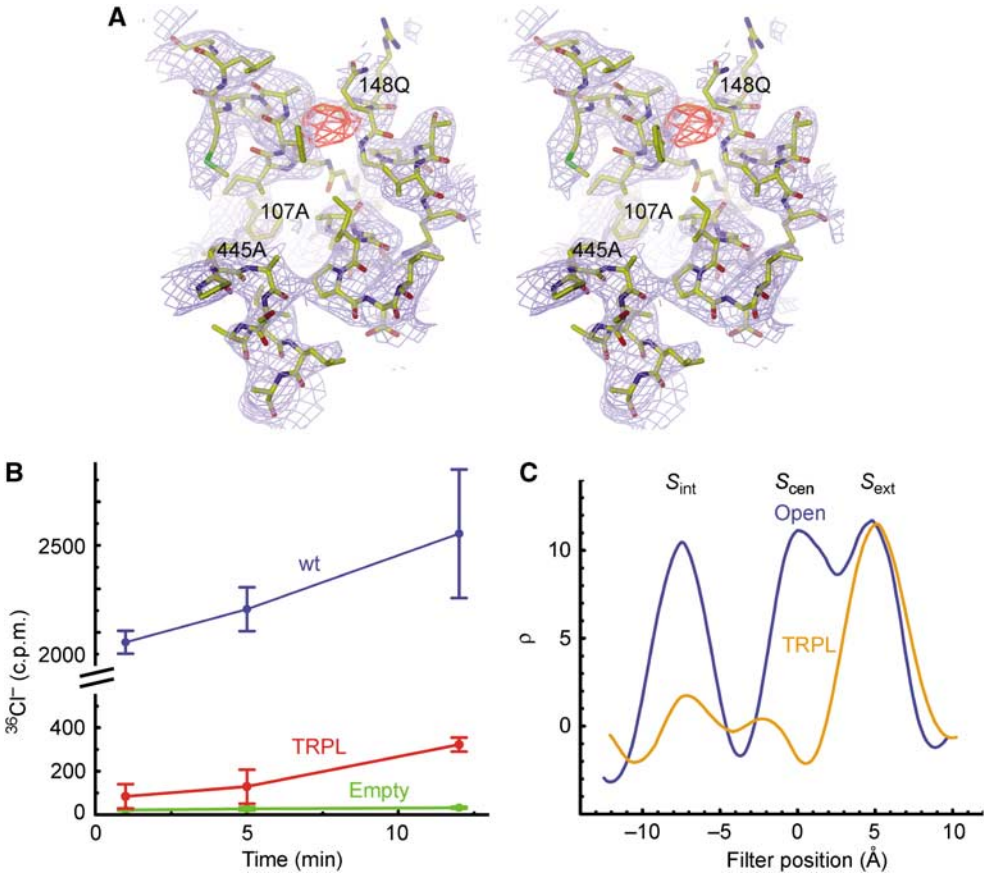

Figure 2 Structure and function of a mutant with a single ion-binding site. (**A**) Stereo view of the selectivity filter of the mutant S107A/E148Q/Y445A (TRPL). The data were collected from a crystal grown in 100 mM Br^-. The view is the same as in Figure 1B. A $2F_o$–F_c electron density map calculated at 3.5 Å resolution and contoured at 1σ is shown superimposed on the refined structure. The Br^- anomalous difference density (red), which was calculated from the same data set, is contoured at 4.5σ. Mutated residues are labeled. (**B**) EcClC-mediated $^{36}Cl^-$ uptake into liposomes. The averages over three data points and the standard deviations are shown. All measurements were carried out at pH 5. The protein was reconstituted at a ratio of 5 μg/mg of lipid. Time courses from vesicles containing wt EcClC and TRPL are shown in blue and red, respectively. Uptake from vesicles without protein is shown in green. (**C**) Anomalous difference electron density in the selectivity filter of TRPL at high Br^- concentration (250 mM). Electron density of the 'open conformation' is shown for comparison.

S_{cen} and S_{int} are 13 and 23 mM, respectively. The ion affinities in the 'closed conformation' differ with respect to the 'open conformation': While the K_D of S_{int} is similar in both conformations, the affinity in S_{cen} is higher in the 'closed conformation' (K_D 5 mM; Figure 3D, Table II). This change in affinity (of about 0.6 kcal/mol) can probably be attributed to small conformational differences in the filter between the 'closed' and the 'open conformation' and to the stronger electrostatic repulsion between two Br^- ions compared to the repulsion between Br^- and the negatively charged glutamate side chain, which can move its negative charge at a larger distance from the ion. It should also be pointed out that by the fit to a single K_D, changes in binding affinity due to the increasing ion occupancy of the neighboring binding sites at higher ion concentrations are neglected. Despite the differences in the observed binding affinities, those changes in partial occupancy will likely play a role for all the three ion-binding sites.

Data collected from crystals of both conformations grown at 1 and 0 mM Br^- allow us to study the structure of the selectivity filter in the absence of bound ions. These structures are determined to an upper resolution between 3.1 and 3.5 Å. Although a detailed investigation of side-chain conformations is not possible at this resolution, larger conformational changes affecting the protein backbone or bulky side chains as Tyr 445 can easily be detected. For both conformations the electron density in the filter and elsewhere is well defined (Supplementary Figure 4). The refined structures are unchanged with respect to their counterparts crystallized at high Br^- concentration (r.m.s.d.$_{all\ atoms}$: 'open conformation' 0.34 Å, 'closed conformation' 0.16 Å), demonstrating that the EcClC selectivity filter retains its integrity even in the absence of bound ions.

Br^-/Cl^- selectivity of the ion-binding sites

To investigate the binding properties of the selectivity filter for Cl^-, we collected data at different Br^-/Cl^- ratios, keeping the total ion concentration in solution at 250 mM (Figure 4A and B). The anomalous difference density decreases with higher Cl^- concentration due to the competition of Cl^- and Br^- for the same binding sites. For the 'open conformation', the decrease in S_{ext} is about linear, reaching half of its size at 50% Br^-; it is steeper in S_{cen} and shallower in S_{int}. The decrease of the signal is indicative for Cl^- binding to all three sites, with affinities comparable to the one observed for Br^-. The electron density in S_{cen} and S_{int} shows similar features in the 'closed conformation' (Figure 3B). The fit of the average electron density to the following equation allows

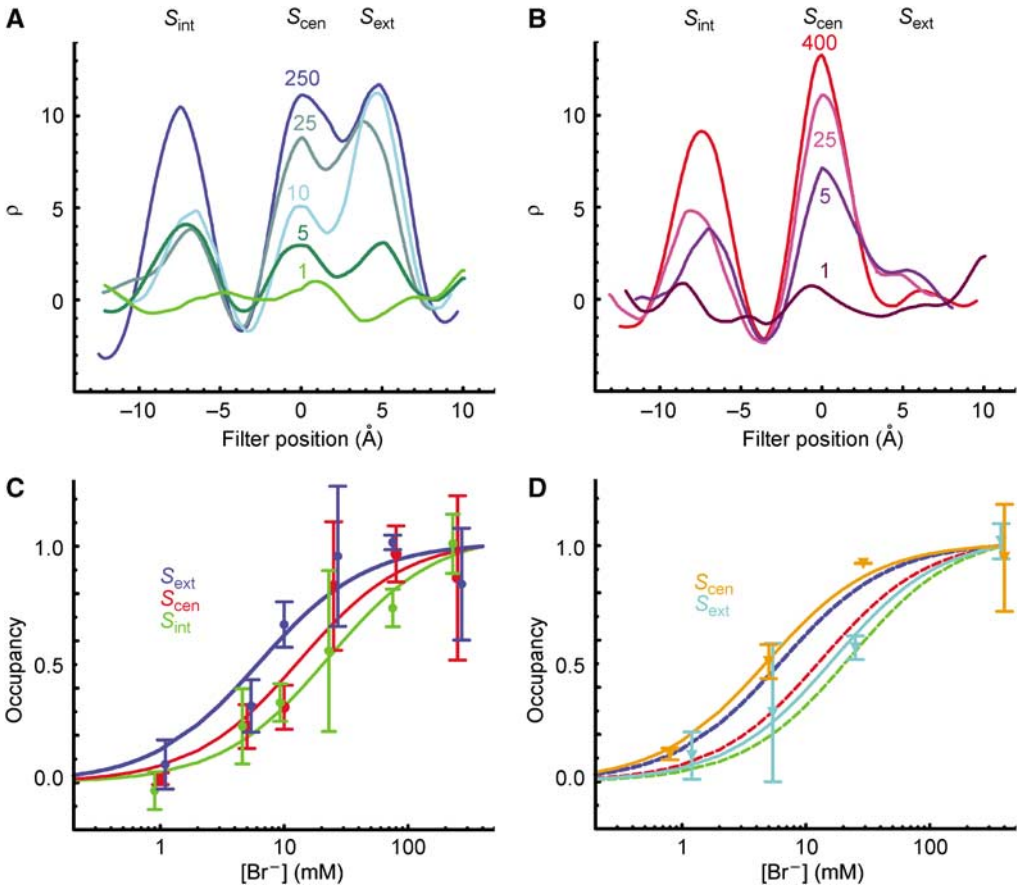

Figure 3 Binding affinity of Br^- to the EcClC selectivity filter. (**A**) Anomalous difference density in the 'open conformation' at different Br^- concentrations. The values refer to the ion concentration in the medium. The traces at different ion concentration have unique colors, with their respective Br^- concentration in mM shown in the same color. The filter position is shown relative to S_{cen}. (**B**) Anomalous difference density in the 'closed conformation' at different Br^- concentrations. (**C**) Br^- affinity in the 'open conformation'. The averages of the peak heights of the electron densities were obtained as described in Table II. The standard deviation (for $n=4$) or the range of values (for $n=2$) is shown as bars. Data for S_{int}, S_{cen} and S_{ext} are colored in green, red and blue, respectively. Curves show a fit of the averaged density to equation (1). Curves, data points and errors were scaled by subtracting ρ_{min} and by subsequently dividing by ($\rho_{max}-\rho_{min}$). (**D**) Br^- affinity in the 'closed conformation'. The data were obtained as described in (C) and is colored in cyan for S_{int} and orange for S_{cen}.

the estimation of the Br^-/Cl^- selectivity and of the Cl^- affinity of the three binding sites (Figure 4C and D, Table II).

$$\rho = \rho_{max}/(1 + K_{DBr^-}/K_{DCl^-} * [Cl^-]/[Br^-]) \qquad (2)$$

The data show little selectivity between Cl^- and Br^- in S_{ext}, slightly higher affinity for Br^- in S_{int} and higher affinity for Cl^- S_{cen} (Table II). Due to the higher Cl^- selectivity of S_{cen}, S_{cen} and S_{ext} appear to bind Cl^- equally well.

Discussion

We have used a crystallographic approach to characterize the ion-binding properties of the ClC Cl^- selectivity filter. This is the first quantitative experimental study of anion binding to an ion-selective transport protein and its results give insight into both functional branches of the ClC family, the gated Cl^- channels and the H^+/Cl^- transporters.

The ClC selectivity filter constitutes a constricted region within the ClC subunit in the center of the membrane. In its 'open conformation', the filter contains three anion-binding sites that bridge the intracellular and extracellular solutions (Figure 1B). Despite their close proximity and the resulting electrostatic repulsion between the bound ions, our data suggest that the filter can accommodate three ions at the same time. The Cl^- ions bind with mM (4–40 mM) affinity. Moreover, ion binding to two of the binding sites (S_{ext} and S_{cen}), which are embedded within the protein, is energetically balanced as the ions bind with similar affinity. This tight energetic balance has been shown to be important for the mechanism of ion conduction in K^+ channels before (Morais-Cabral *et al*, 2001). The ion in the intracellular site S_{int} is still partly in contact with the solution and binds with lower affinity (Table II). The three sites are only moderately selective for Cl^-/Br^-. This moderate selectivity probably reflects the fact that only Cl^- plays a role as permeant anion in biological systems.

The determined ion affinities have potential consequences for the ion occupancy under physiological conditions. In a cellular environment, the binding sites S_{int} and S_{cen} are in the 'closed conformation' only, exposed to the low intracellular Cl^- concentration (~5 mM in muscle cells, and up to 40 mM in certain other cells). At this low physiological concentration S_{cen} would still be occupied, whereas S_{int} would mostly be empty. Only upon opening and facing the high extracellular Cl^- concentration, all three binding sites become occupied. This result is interesting in light of the contribution of the

Table II Average anomalous difference density[a]

Br^- conc.	S_{int}	S_{cen}	S_{ext}	No. of data sets
'Open conformation' affinity				
0 mM	1.9±0.7	2.3±0.4	2.0±0.4	2
1 mM	0.9±0.7	1.0±0.3	1.6±1.4	2
5 mM	3.3±1.5	3.6±1.1	5.0±1.6	2
10 mM	4.2±0.7	4.6±1.1	9.6±1.3	2
25 mM	6.1±3.1	10.6±3.3	13.5±4.0	2
75 mM	7.7±0.7	12.3±1.5	14.3±0.4	1
250 mM	10.1±1.1	11.0±4.1	11.9±3.2	2
'Closed conformation' affinity				
1 mM	1.5±0.8	1.0±0.3	—	1
5 mM	2.9±0.9	5.9±0.9	—	2
25 mM	5.1±0.4	11.1±0.0	—	1
400 mM	8.7±0.6	11.4±2.7	—	1
TRPL	—	—	10.2±1.8	2
'Open conformation' selectivity[b]				
75% Br^-	7.7±2.3	4.1±1.6	8.1±2.7	2
50% Br^-	6.6±1.0	2.0±1.6	4.0±0.9	2
25% Br^-	3.0±0.6	1.4±0.8	2.8±0.9	2
'Closed conformation' selectivity[b]				
75% Br^-	10.0±0.1	6.8±0.8	—	1
50% Br^-	5.4±0.0	3.5±0.1	—	1
25% Br^-	3.2±1.1	2.1±0.8	—	1

	'Open conformation'		'Closed conformation'	
	K_{DBr^-} (mM)	K_{DBr^-}/K_{DCl^-}	K_{DBr^-} (mM)	K_{DBr^-}/K_{DCl^-}
Affinities/selectivities[c]				
S_{int}	22.8	0.67	16.8	0.57
S_{cen}	13.3	4.3	4.8	2.0
S_{ext}	6.2	1.6	—	—

[a]The respective peak heights of the binding sites S_{int}, S_{cen} and S_{ext} are averaged between the two subunits in the asymmetric unit and between different data sets (Table I). The averages and the standard deviations are listed.
[b]For the 'open conformation' and 'closed conformation' selectivity experiments, the Br^- concentration in solution is given in % of a combined $Cl^- + Br^-$ concentration of 250 mM.
[c]Br^- affinities and Br^-/Cl^- selectivities were obtained from a fit of the peak heights to equations (1) and (2), respectively.

ions to the voltage dependence of gating in some ClC channels, and in light of the 2:1 stoichiometry for Br^- to H^+ in the transporters (Pusch *et al*, 1995; Chen and Miller, 1996; Accardi and Miller, 2004).

Our results are in qualitative agreement with a theoretical study employing continuum electrostatics to analyze the interaction of the ions with the protein. The calculations reveal that this region is strongly electropositive and is able to accommodate three ions at a time (Faraldo-Gomez and Roux, 2004). In absolute terms, however, the estimated binding energies for S_{ext} and S_{int} of 7–8 kcal/mol would cause a binding affinity in the low μM range, which is considerably larger than the experimentally determined values.

Ion transporters and ion channels have traditionally been viewed to be constructed by very different protein architectures. While this holds true for the majority of channels and transporters, the ClC family is an exception, where a very similar conserved molecular framework encodes for gated ion channel ion transporters. In light of this strong conservation, we propose that the structure of the secondary ion transporter EcClC resembles the structure of ClC channels with respect to ion binding. For this reason, it is interesting to compare the ion-binding data from this study with experimental data on the well-characterized ClC channels ClC-0 and ClC-1. Several experiments have previously addressed the question whether ClC channels are single- or multi-ion pores. Due to the saturation of conductance at high Cl^- concentration, an early study suggested that ClC-0 might be a single-ion pore, although with several ion-binding sites in the filter (Figure 5A) (White and Miller, 1981). Later studies, however, which analyzed the anomalous mole fraction behavior in binary mixtures of ions for ClC-0 and ClC-1, were more compatible with a multiply occupied selectivity filter (Figure 5B) (Pusch *et al*, 1995; Fahlke *et al*, 1996; Rychkov *et al*, 1998). Our study now confirms that the filter, indeed, shows multiple occupancy of ions. The saturation of conductance with Cl^- concentration allows a comparison of the ion-binding affinities. For ClC-1, the conductance saturates with an apparent K_D of 5 mM for Cl^- influx and of 35 mM for Cl^- efflux (Rychkov *et al*, 1998). Similarly, in ClC-0, Cl^- efflux was shown to saturate with an apparent K_D of 59 mM (Chen and Chen, 2003). These results are in striking agreement with the affinity data measured for EcClC in this study (K_D for Cl^-: $S_{ext} = 4$–6 mM, $S_{int} = 34$–46 mM), indicating that the physico-chemical properties of the selectivity filter are conserved within the ClC family. Ion permeation in ClC channels might consequently work as outlined in Figure 5B: A queue of ions occupies the selectivity filter in the open state of a ClC channel. Additional ions, which enter the filter from either side of the membrane, cause the bound ions to move in a single file towards the next binding site. This movement leads to the dissociation of the ion on the juxtaposed side of the queue into the aqueous vestibule. Mutual repulsion between the ions and a relay of interactions within the selectivity filter will lower the energy barriers when moving between ion-binding sites.

Unexpectedly, the EcClC structure has currently told us more about the function of the ClC channels than about the transporters within the family. Our data do not explain the mechanism of coupling of H^+ and Cl^- ions in EcClC. The conservation of ion binding between the transporter EcClC and the ClC channels, and the role of the conserved glutamate residue in gating and transport, however, emphasizes the close relationship between the two mechanisms, permeation and gating and coupled transport within the family. The detailed knowledge of the ion-binding properties of EcClC selectivity filter will certainly provide a good foundation for future studies on the transport cycle involving site-directed mutants.

When comparing the ion permeation mechanisms of K^+ and Cl^- channels, common motives but also differences become apparent. Some of the properties such as the molecular architecture of the protein, the chemistry of ion binding and the mechanisms of gating have been discussed previously (Dutzler *et al*, 2002, 2003; Dutzler, 2004). With the results of this study, we can now compare additional features. Both K^+ channels and Cl^- channels are multi-ion pores, which use the mutual repulsion between neighboring ions to lower the barriers for ions diffusing through the channel (Morais-Cabral *et al*, 2001; Zhou and MacKinnon, 2003). It is interesting to note that in K^+ channels the four consecutive ion-binding sites are never fully occupied by K^+; it is

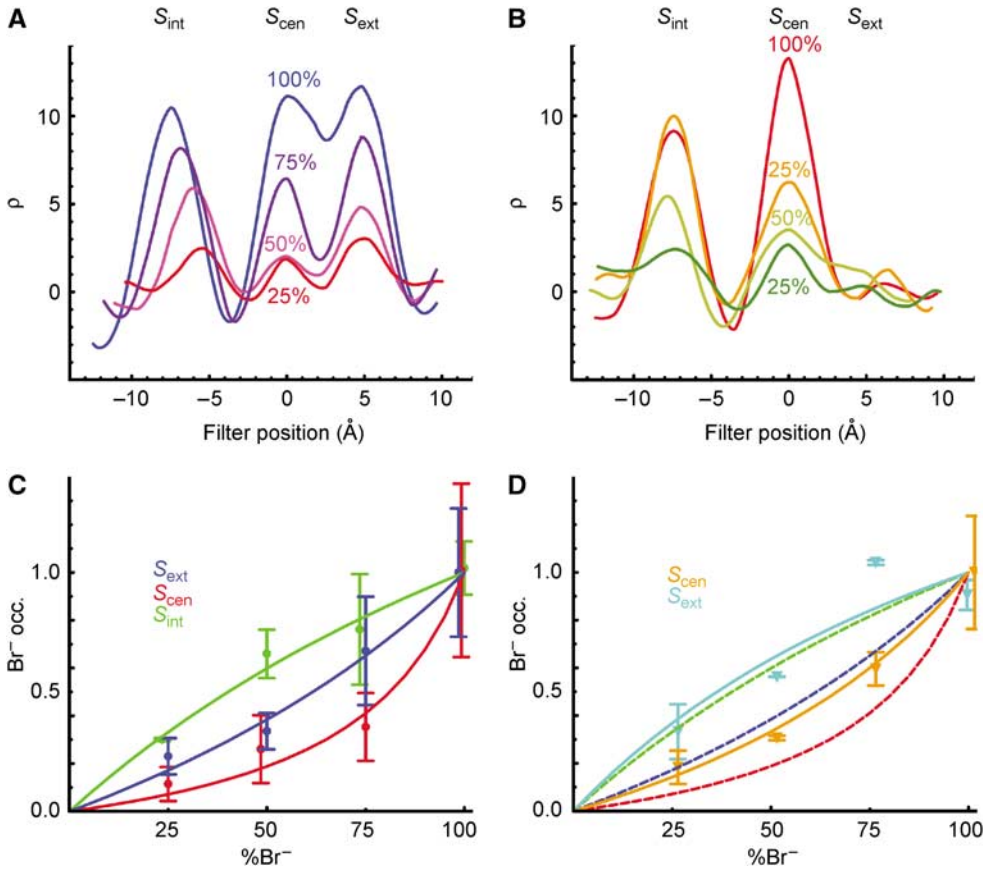

Figure 4 Br^-/Cl^- selectivity in the EcClC selectivity filter. (**A**) Anomalous difference density in the 'open conformation' at different Br^-/Cl^- ratios. The total halide ion concentration in solution is in all cases 250 mM. The data sets are colored in unique colors and labeled with the respective Br^- ratio. The filter position is shown relative to S_{cen}. (**B**) Anomalous difference density in the 'closed conformation' at different Br^-/Cl^- ratios. The Br^- ion concentration at 100% Br^- is 400 mM; in all other cases the total halide concentration is 250 mM. (**C**) Br^-/Cl^- selectivity in the 'open conformation'. The averages of the peak heights of the electron densities were obtained as described in Table II. The standard deviation (for $n=4$) or the range of values (for $n=2$) is shown as bars. Data for S_{int}, S_{cen} and S_{ext} are colored in green, red and blue, respectively. Curves show a fit of the averaged density to equation (2). Curves, data points and errors were scaled by dividing by (ρ_{max}). (**D**) Br^- affinity in the 'closed conformation'. The data were obtained as described in (C) and are colored in cyan for S_{int} and orange for S_{cen}.

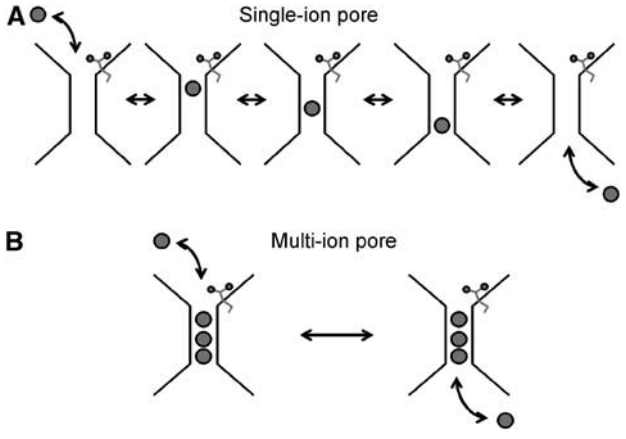

Figure 5 Two models for ion conduction. Schematic drawing of ion conduction in a single ion pore and a multiple-ion pore. (**A**) Single-ion pore: The selectivity filter binds only one ion at a time. During permeation the ion enters the selectivity filter from the solution and diffuses between the different binding sites of the channels until it dissociated from the filter. (**B**) Multiple-ion pore: The selectivity filter binds multiple ions, which permeate in a single file when additional ions enter the filter. The filter is depicted in its open state; the ions are drawn as spheres.

rather a single file of alternating K^+ ions and water molecules binding to the K^+ selectivity filter (Morais-Cabral *et al*, 2001; Zhou and MacKinnon, 2003). In contrast to K^+ channels, our data suggest that the binding sites in the ClC Cl^- selectivity filter are indeed fully occupied. As in K^+ channels, energetic balance between the binding sites might contribute to a larger ion permeation rate.

Another difference between the two selectivity filters is found at low ion concentration. The K^+ channel selectivity filter undergoes a conformational change into a nonconducting conformation when the K^+ concentration is lowered to 3 mM. It was proposed that the energy required to change the selectivity filter into a conducting conformation in K^+ channels weakens its affinity for the ion and contributes therefore to an increased conduction rate (Zhou *et al*, 2001; Zhou and MacKinnon, 2003). The ClC selectivity filter does not undergo a similar conformational change; it retains its conformation even in the absence of bound ions, which could contribute to the generally lower conduction rates observed in ClC channels when compared to K^+ channels.

With K^+ channels and Cl^- channels, nature evolved different molecular frameworks for selective ion channel proteins. Despite the structural differences it is striking to find similar principles, which govern ion conduction. Next to

the similarities, however, there are also differences, which probably reflect the unique chemical features of the permeating ions, and the tight energetic balance that has to be maintained to allow the diffusion of ions at high rates through the channel.

Materials and methods

Protein preparation

Wt EcClC and the EcClC mutant E148Q were expressed and purified in the detergent decyl maltoside (DM) as described (Dutzler *et al*, 2002). Mouse IGG was purified from mouse hybridoma cell culture and Fab fragments were obtained as described (Dutzler *et al*, 2003). EcClC and Fab were mixed in an OD_{280} ratio of 1:1.5. The complex was purified on a Superdex 200 column (Pharmacia) equilibrated in 10 mM Tris (pH 7.5), 10 mM DM and 150 mM NaBr. Protein used for crystallization in the absence of Br^- and Cl^- was purified in 150 mM Na^+/K^+ tartrate instead of NaBr. Peak fractions containing the EcClC–Fab complex were pooled and concentrated to a final concentration of 15 mg/ml (Millipore). For crystallization in different ion compositions, aliquots of the protein were dialyzed against a solution containing 10 mM DM, 10 mM Tris, and 100 mM NaCl, 100 mM NaBr or 100 mM Na^+/K^+ tartrate.

Crystal preparation

Crystals of the EcClC–Fab complex were grown in sitting drops at 20°C by equilibrating a 1:1 mixture of protein and reservoir solution against the reservoir. Careful measurements of the drop volume of the mixture after equilibration showed a decrease in the volume towards the volume of the initially added precipitant solution. We therefore used the following convention for the ion concentration in the crystallization solution: The Br^- concentration present in the protein solution and the crystallization solution are summed up to the total ion concentration in solution. This is justified since the drops are equilibrated upon harvesting of the crystals. Two crystal forms were used for this study. For both crystal forms, crystals were grown in a pH range between 6.5 and 9.5. The pH did not have any observable influence on the protein conformation or the ion-binding properties. The buffers used for crystallization are: ADA (pH 6.5), Hepes (pH 7.5), Tris (pH 8.5) and glycine (pH 9.5). For the high-halide crystal form (250–400 mM Br^-or Cl^-), protein dialyzed into Br^- was mixed with reservoir solution containing 33–38% Peg200/Peg300 (in a 1:2 v/v ratio), 150–300 mM Br^- and 50 mM buffer at the respective pH. For Br^-/Cl^- titrations, proteins dialyzed against a solution containing either 100 mM NaBr or 100 mM NaCl were mixed in the desired ratio. Crystals were grown by using a precipitant concentration containing NaBr and NaCl in the same ratio at a total concentration of 150 mM. For the low-halide crystal form (0–75 mM Br), NaBr was added to the protein solution previously dialyzed against 100 mM Na^+/K^+ tartrate at the desired final concentration. Crystals were grown by mixing with a reservoir solution containing 35–40% Peg200/Peg300 (in a 1:2 v/v ratio), 150 mM Na^+/K^+ tartrate and 50 mM buffer at the respective pH. The crystals were frozen in their mother liquor by rapid transfer into liquid propane.

Data collection and crystallographic analysis

All data sets were collected on frozen crystals on a Mar CCD detector at the X06SA beamline at the Swiss Light Source (SLS) of the Paul Scherrer Institute (PSI). For collecting anomalous differences, the wavelength was set to the Br^- K-edge (0.92 Å). The data were indexed and integrated with DENZO and SCALEPACK (Otwinowski and Minor, 1997) and further processed with CCP4 programs (CCP4, 1994). All crystals of the high-halide crystal form are of space group *C2* ($a = 230$ Å, $b = 94$ Å, $c = 169$ Å, $\alpha = \gamma = 90°$, $\beta = 131.5°$), with one ClC dimer and two Fab fragments in the asymmetric unit. The structures of the wt EcClC–Fab complex 1OTS and of the mutant complex EcClC–E148Q–Fab 1OTU served as starting models (Dutzler *et al*, 2003). Ions and water molecules were removed previously. Refinement was initiated by several cycles of rigid body refinement with CNS, followed by cycles of minimization (Brunger *et al*, 1998). The phases were improved by solvent flattening and two-fold domain-averaging breaking the complex structure into three domains (channel, F_v region, F_c region) in DM (Cowtan, 1994). Structures and electron densities were inspected with the program O (Jones *et al*, 1991). The structures were adjusted manually if required. R_{free} was monitored throughout the refinement. All crystals of the low-halide crystal form are of space group *C2* ($a = 220$ Å, $b = 120$ Å, $c = 150$ Å, $\alpha = \gamma = 90°$, $\beta = 128°$), with one ClC dimer and two Fab fragments in the asymmetric unit. The structures were solved by molecular replacement using the respective structures 1OTS and 1OTU as search models (Navaza, 2001). Refinement was continued as described for the high-halide crystal form. For both crystal forms, the anomalous difference maps were calculated with CCP4 programs. Ions were not included in the model for calculating the phases. The maps were normalized and a one-dimensional density profile along the pore was sampled using the program MAPMAN (Kleywegt and Jones, 1994). In an alternative approach, the data sets were first scaled to the highest resolution data set of the respective crystal form and the electron distribution was subsequently sampled without normalization. The density obtained this way was found to have features similar to the normalized difference density maps (Supplementary Figure 1D). For the calculation of the anomalous difference densities, a high-resolution cutoff of $I/\sigma I > 5$ was used throughout. Fluctuations in the peak heights between data sets of the same ion concentration are probably due to the difference in data quality and the stability of the wavelength during data collection.

Concentrative $^{36}Cl^-$ uptake assay

Influx of $^{36}Cl^-$ into liposomes was essentially carried out as described (Maduke *et al*, 1999; Accardi *et al*, 2004). Wt EcClC and the mutant S107A/E148A/Y445A have been purified as described (Dutzler *et al*, 2002), with the exception that the gel filtration step was replaced by purification on a cation exchange column (MonoS Pharmacia). The protein was subsequently reconstituted into liposomes in a ratio of 5 μg of protein per mg of lipid (*E. coli* polar lipids Avanti). For the negative control, vesicles were reconstituted without addition of protein. Uptake was studied at pH 5 at an intravesicular Cl^- concentration of 450 mM. The uptake was initiated by adding 1 mM Cl^- (containing 0.4 μCi of $^{36}Cl^-$ per ml of vesicle suspension) to the extravesicular solution. At desired times samples were collected by adding 100 μl of liposomes to a Dowex-glutamate column. The vesicles were eluted in 1.5 ml of 400 mM sorbitol. In all, 14.5 ml of scintillation liquid was added and the radioactivity was counted on a Betamatic 2 scintillation counter (Kontron).

Supplementary data

Supplementary data are available at *The EMBO Journal* Online.

Acknowledgements

We are grateful to the staff of the X06SA beamline for their support during data collection, Mike Walden for his help on the transport assay and members of the Dutzler lab for support at all stages of the project. The antibody binding to EcClC was produced at the National Cell Culture Center (NCCC) in Minneapolis, MN, USA. Data collection was performed at the Swiss Light Source (SLS) of the Paul Scherrer Institute (PSI). This work was supported by a grant from the Swiss National Science Foundation (SNSF) and the NCCR Structural Biology program. We declare that we have no competing financial interest. The novel structures resulting from this study have been deposited with the Protein Data Bank under the accession codes 2EXW, 2EXY and 2EZ0.

References

Accardi A, Kolmakova-Partensky L, Williams C, Miller C (2004) Ionic currents mediated by a prokaryotic homologue of CLC Cl− channels. *J Gen Physiol* **123:** 109–119

Accardi A, Miller C (2004) Secondary active transport mediated by a prokaryotic homologue of ClC Cl− channels. *Nature* **427:** 803–807

Brunger AT, Adams PD, Clore GM, DeLano WL, Gros P, Grosse-Kunstleve RW, Jiang JS, Kuszewski J, Nilges M, Pannu NS, Read RJ, Rice LM, Simonson T, Warren GL (1998) Crystallography & NMR system: a new software suite for macromolecular structure determination. *Acta Crystallogr D* **54** (Part 5)**:** 905–921

CCP4 (1994) Collaborative Computational Project Nr. 4. The CCP4 Suite: programs for X-ray crystallography. *Acta Crystallogr D* **50:** 760–763

Chen MF, Chen TY (2003) Side-chain charge effects and conductance determinants in the pore of ClC-0 chloride channels. *J Gen Physiol* **122:** 133–145

Chen TY, Miller C (1996) Nonequilibrium gating and voltage dependence of the ClC-0 Cl− channel. *J Gen Physiol* **108:** 237–250

Cowtan K (1994) An automated procedure for phase improvement by density modification. *Jt CCP4 ESF-EACBM Newslett Prot Crystallogr* **31:** 34–38

Doyle DA, Morais Cabral J, Pfuetzner RA, Kuo A, Gulbis JM, Cohen SL, Chait BT, MacKinnon R (1998) The structure of the potassium channel: molecular basis of K+ conduction and selectivity. *Science* **280:** 69–77

Dutzler R (2004) Structural basis for ion conduction and gating in ClC chloride channels. *FEBS Lett* **564:** 229–233

Dutzler R, Campbell EB, Cadene M, Chait BT, MacKinnon R (2002) X-ray structure of a ClC chloride channel at 3.0 A reveals the molecular basis of anion selectivity. *Nature* **415:** 287–294

Dutzler R, Campbell EB, MacKinnon R (2003) Gating the selectivity filter in ClC chloride channels. *Science* **300:** 108–112

Engh AM, Maduke M (2005) Cysteine accessibility in ClC-0 supports conservation of the ClC intracellular vestibule. *J Gen Physiol* **125:** 601–617

Estevez R, Schroeder BC, Accardi A, Jentsch TJ, Pusch M (2003) Conservation of chloride channel structure revealed by an inhibitor binding site in ClC-1. *Neuron* **38:** 47–59

Fahlke C, Rosenbohm A, Mitrovic N, George Jr AL, Rudel R (1996) Mechanism of voltage-dependent gating in skeletal muscle chloride channels. *Biophys J* **71:** 695–706

Faraldo-Gomez JD, Roux B (2004) Electrostatics of ion stabilization in a ClC chloride channel homologue from *Escherichia coli*. *J Mol Biol* **339:** 981–1000

Hille B, Schwarz W (1978) Potassium channels as multi-ion single-file pores. *J Gen Physiol* **72:** 409–442

Jentsch TJ, Stein V, Weinreich F, Zdebik AA (2002) Molecular structure and physiological function of chloride channels. *Physiol Rev* **82:** 503–568

Jones TA, Zou JY, Cowan SW, Kjeldgaard M (1991) Improved methods for building protein models in electron density maps and the location of errors in these models. *Acta Crystallogr A* **47** (Part 2)**:** 110–119

Kleywegt G, Jones TA (1994) In *CCP4 Study Weekend*, Bailey S, Hubbard R, Waller D (eds), pp 59–66. Daresbury, UK: Daresbury Laboratory

Maduke M, Pheasant DJ, Miller C (1999) High-level expression, functional reconstitution, and quaternary structure of a prokaryotic ClC-type chloride channel. *J Gen Physiol* **114:** 713–722

Morais-Cabral JH, Zhou Y, MacKinnon R (2001) Energetic optimization of ion conduction rate by the K^+ selectivity filter. *Nature* **414:** 37–42

Navaza J (2001) Implementation of molecular replacement in AMoRe. *Acta Crystallogr D* **57:** 1367–1372

Otwinowski Z, Minor W (1997) Processing of X-ray diffraction data collected in oscillation mode. *Methods Enzymol* **267:** 307–326

Parsegian A (1969) Energy of an ion crossing a low dielectric membrane: solutions to four relevant electrostatic problems. *Nature* **221:** 844–846

Picollo A, Pusch M (2005) Chloride/proton antiporter activity of mammalian CLC proteins ClC-4 and ClC-5. *Nature* **436:** 420–423

Pusch M, Ludewig U, Rehfeldt A, Jentsch TJ (1995) Gating of the voltage-dependent chloride channel CIC-0 by the permeant anion. *Nature* **373:** 527–531

Rychkov GY, Pusch M, Roberts ML, Jentsch TJ, Bretag AH (1998) Permeation and block of the skeletal muscle chloride channel, ClC-1, by foreign anions. *J Gen Physiol* **111:** 653–665

Scheel O, Zdebik AA, Lourdel S, Jentsch TJ (2005) Voltage-dependent electrogenic chloride/proton exchange by endosomal CLC proteins. *Nature* **436:** 424–427

Traverso S, Elia L, Pusch M (2003) Gating competence of constitutively open CLC-0 mutants revealed by the interaction with a small organic inhibitor. *J Gen Physiol* **122:** 295–306

White MM, Miller C (1979) A voltage-gated anion channel from the electric organ of *Torpedo californica*. *J Biol Chem* **254:** 10161–10166

White MM, Miller C (1981) Probes of the conduction process of a voltage-gated Cl− channel from *Torpedo electroplax*. *J Gen Physiol* **78:** 1–18

Zhou Y, MacKinnon R (2003) The occupancy of ions in the K^+ selectivity filter: charge balance and coupling of ion binding to a protein conformational change underlie high conduction rates. *J Mol Biol* **333:** 965–975

Zhou Y, MacKinnon R (2004) Ion binding affinity in the cavity of the KcsA potassium channel. *Biochemistry* **43:** 4978–4982

Zhou Y, Morais-Cabral JH, Kaufman A, MacKinnon R (2001) Chemistry of ion coordination and hydration revealed by a K^+ channel–Fab complex at 2.0 A resolution. *Nature* **414:** 43–48